Proceedings of the Canadian Society for Mechanical Engineering International Congress
32nd Annual Conference of the Computational Fluid Dynamics Society of Canada
Canadian Society of Rheology Symposium
CSME/CFDSC/CSR 2025
May 25–28, 2025, Montréal, Québec, Canada

Scale-Resolving Simulation of a Water Jet Pump

Akbar Ravan Ghalati[1,2*], Hakim Nesreddine[3], Jay Lacey[1], Sébastien Poncet[2]

[1]Civil engineering Department, Université de Sherbrooke, Sherbrooke, Canada
[2]Mechanical engineering Department, Université de Sherbrooke, Sherbrooke, Canada
[3]Laboratoire des technologies de l'énergie, Hydro-Québec, Shawinigan, Canada
*Akbar.Ravan.Ghalati@USherbrooke.ca

***Abstract*—**Jet pumps are versatile hydraulic devices designed for displacing and/or mixing fluids. Scale-Resolving Simulations (SRS) of jet pumps are prohibitively expensive due to the presence of high Reynolds number flows and complex interactions within a wall-bounded domain. This study evaluates three SRS models to identify the most suitable approach for efficiently capturing the internal flow dynamics of jet pumps. Comparisons with experimental data reveal that while Stress-Blended Eddy Simulation (SBES) provides results comparable to Wall-Adapting Local Eddy-Viscosity (WALE) and Algebraic Wall-Modeled LES (AWMLES), it requires significantly lower computational costs. Simulation of the jet pump at various flow ratios (0.5, 1.6, and 2.16) revealed that as the flow ratio increases, the location where the primary jet breaks up due to momentum transfer with the secondary flow shifts further downstream. This finding is particularly important when the jet pump is used as a mixer, as mixing a larger amount of secondary flow with a constant amount of primary flow requires a longer device to ensure effectiveness.

***Keywords-component*—Jet Pump; Stress-Blended Eddy Simulation; Large Eddy Simulation; mixing.**

I. Introduction

The Jet pump is a passive pumping devices which can be utilized for pressurizing and/or displacing various fluids. It operate based on the energy of a primary fluid and consists of four main components, namely: nozzle, suction chamber, mixing throat and diffuser. Discharging the primary fluid into the mixing throat through a nozzle forms a low-pressure region at the beginning of the mixing section. The created vacuum forces the secondary fluid into the pump. In the mixing throat, the primary fluid will transfer part of its kinetic energy to the secondary fluid while the two flows are mixing together. Then the mixed fluid is introduced into the diffuser where its pressure is gradually increased [1].

Jet pumps have been employed in various applications, including mixing fluids [2], silt removal operations [3], deep-sea aquaculture system [4], refrigeration systems [5], desalination of sea water [6] and conveying fish [7], to name a few. While they offer advantages such as high reliability, low operational costs, and compatibility with diverse working fluids, their design and performance prediction remain challenging due to the existence of complex internal flow field [8].

Experimental analyses of jet pumps have mostly focused on global measurement techniques, which involve recording parameters such as pressure and flow rate to quantify the device's performance [9]–[12]. While these methods provide necessary insights, they are limited in capturing the intricate details of the complex internal flow field.

With increasing power of computational resources, Computational Fluid Dynamics (CFD) has become an indispensable tool for investigating the complex flow phenomena within jet pumps. Among the various CFD approaches, the Reynolds-Averaged Navier-Stokes (RANS) method is a widely used technique for simulating jet pumps' flow field. This approach was used to explore the effects of geometrical (e.g. in [13]) and operational parameters (e.g. in [14]) on jet pump performance. Yang and Long [15] compared the performance of six turbulence models, including the three $k-\varepsilon$ variations (Standard, RNG and Realizable), the standard and SST $k-\omega$, and Reynolds Stress Models (RSM), in capturing the flow field of water jet pumps. Their study found no significant differences between the models' predictions when the jet pump operated at a low flow ratio (the ratio of secondary to primary flow rates). It was also mentioned that modifying the turbulence model constants reduced the difference between experimental and numerical data. While RANS approach decently provides a time-averaged representation of the flow field, this method does not capture the turbulent structures which play a critical

role in processes like mixing [17]–[19]. Xu et al. [20] used Large Eddy Simulations (LES) along with the Smagorinsky sub-grid scale model to investigate the internal flow field of an annular jet pump. The instantaneous velocity field showed that decreasing the flow ratio leads to the occurrence of a re-circulation region in the suction chamber. It was also reported that the spanwise vorticity magnitude is higher than that of the streamwise in the annular jet pump. In another study, Xu et al. [21] investigated the effects of operational and geometrical parameters on coherent structures of an annular jet pump using various criteria including the pressure, vorticity and Q-criterion. It was concluded that the jet pump with higher area ratio experiences higher vortex shedding frequency. Zaheer and Masud [22] selected the Embeded LES method available in Ansys Fluent for visualizing various types of coherent structures inside a liquid ejector pump. The breaking up of large vortices into smaller ones was introduced as the physics behind enhanced mixing in the device.

Given the high computational cost of LES simulations for jet pumps due to their typically high Reynolds number, this study first evaluates the performance of three Scale-Resolving CFD models, namely Wall-Adapting Local Eddy-Viscosity (WALE), Algebraic Wall-Modeled LES (AWMLES) and Stress-Blended Eddy Simulation (SBES), to identify the most suitable approach for efficiently capturing the complex internal flow dynamics of the jet pump. Once the optimal model is selected, it is utilized to investigate the behavior of the internal flow field across various flow ratios.

The outline of the paper is as follows. Section II presents the methodology, and Section III provides details of the numerical domain. Section IV covers the results and their interpretation, while Section V summarizes the key findings of the present investigation.

II. Methodology

The procedure of filtering the Navier-Stokes equations results in additional subgrid-scale stresses (SGS), which are commonly modeled using the Boussinesq hypothesis. This approach relates the SGS tensor to the resolved strain rate via an eddy viscosity, μ_t. The eddy viscosity is determined based on the employed turbulence model. The formulations of the three Scale-Resolving CFD models used in this study, namely WALE, AWMLES, and SBES, are provided below. Details of the numerical solution, including spatial and temporal discretization, pressure-velocity coupling, and the time-averaging process, are discussed in Subsection II-D.

A. WALE turbulence model

The WALE model is designed to return the correct wall asymptotic (y^3) behavior for wall bounded flows [23] and a zero turbulent viscosity for laminar regions. The eddy viscosity is modelled by Eq. 1:

$$\mu_t = \rho L_s^2 \frac{(S_{ij}^d S_{ij}^d)^{3/2}}{(\bar{S_{ij}}\bar{S_{ij}})^{5/2} + (S_{ij}^d S_{ij}^d)^{5/4}} \tag{1}$$

where ρ is the fluid density, and $\bar{S_{ij}}$ is the rate-of-strain tensor for the resolved scales defined by Eq. 2. L_s and S_{ij}^d are defined by Eqs 3 and 4, respectively.

$$\bar{S_{ij}} = \frac{1}{2}(\frac{\partial \bar{u_i}}{\partial x_j} + \frac{\partial \bar{u_j}}{\partial x_i}) \tag{2}$$

$$L_s = min(\kappa d, C_W \Delta) \tag{3}$$

$$S_{ij}^d = \frac{1}{2}(\bar{g}_{ij}^2 + \bar{g}_{ji}^2) - \frac{1}{3}\delta_{ij}\bar{g}_{kk}^2 \tag{4}$$

where κ=0.41 is the von Kármán constant, d is the distance to the closest wall, C_W=0.325, $\Delta = V^{1/3}$ where V is the volume of the computational cell and $\bar{g}_{ij} = \frac{\partial \bar{u_i}}{\partial x_j}$.

B. AWMLES turbulence model

The subgrid-scale turbulent viscosity in AWMLES [24] is modelled by:

$$\mu_t = \rho \cdot \min\left[(\kappa d)^2, (C_{\text{smag}}\Delta)^2\right] \cdot S \cdot \left\{1 - \exp\left[-\left(\frac{y^+}{25}\right)^3\right]\right\} \tag{5}$$

where S is the magnitude of the strain tensor, C_{smag}=0.2 and $y^+ = d(\sqrt{\tau_w/\rho})/\nu$ is the non-dimensional wall distance (τ_w is the wall shear stress and ν the fluid kinematic viscosity).

C. SBES turbulence model

SBES is a hybrid RANS-LES turbulence model which was introduced in [25] to address industrial requirements for a more modular turbulence modeling approach than Detached Eddy Simulation (DES) family. It also offers a clear distinction between RANS and LES regions while ensuring strong boundary layer shielding and rapid transition to resolved turbulence in separating shear layers. In this approach, the pre-selected RANS and LES models are blended via a shielding function (f_s) in the following way:

$$\tau_{ij} = \tau_{ij}^{RANS} f_s + \tau_{ij}^{LES}(1 - f_s) \tag{6}$$

In the present work, the Realizable $k-\varepsilon$ [26] is used as RANS model, and the WALE model [23] is adopted for the LES part.

D. Solution Strategy

The governing equations for the conservation of mass, momentum and turbulence are solved using a control-volume-based technique that consists of discretization of the integral governing equation on the computational grid and linearization of the discretized equations. The spatial discretization is achieved by Bounded Central Difference, while a second-order method is used for the calculation of pressure at the cell faces. k and ε equations (which only exist in SBES model) are discretized using Second Order Upwind. Additionally, the transient terms are discretized by Implicit Second Order method. The gradients of all variables are computed based

on Least Squares Cell-Based gradient method. The mass flux through the cell faces is calculated using the Rhie-Chow method, and the Coupled algorithm is selected to overcome the pressure-velocity coupling. Finally, the obtained linear system of equations is solved by the Gauss-Seidel method. The averaged results were achieved during the 0.75 s sampling period with a time step of 10^{-5} s.

III. Numerical Domain

Fig. 1 depicts the numerical domain along with the location of boundary conditions. The domain is designed based on the jet pump used in the experiments of Sanger [27], which used water for both the primary and secondary flows. Based on the experiments, the mass flow rate of 3.97 kg/s and the pressure of 103kPa are fixed on the primary inlet and secondary inlet, respectively. The mass flow rate of the outlet is changed to achieve various flow ratios. The area ratio (ratio of the primary nozzle area to the mixing throat area) of the selected jet pump is 0.197 and there is no space between the primary nozzle outlet and the mixing throat.

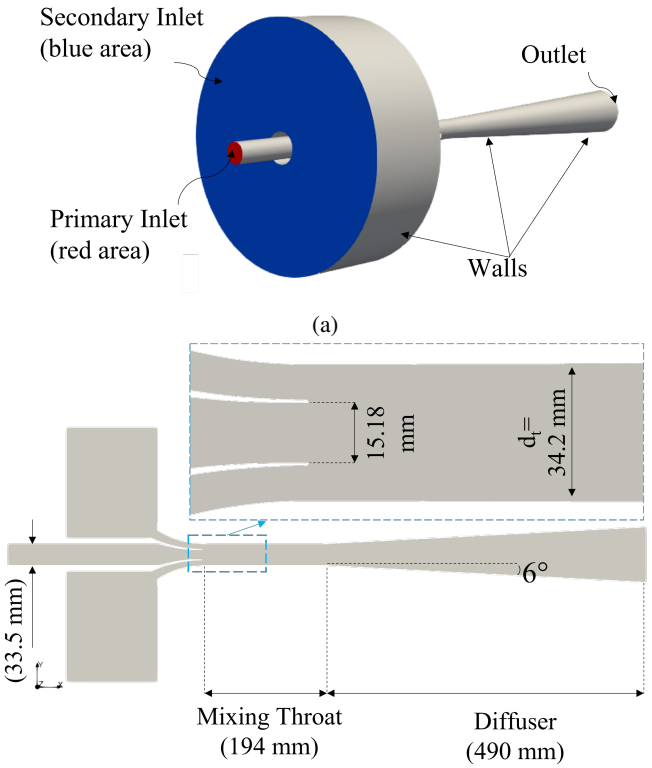

Figure. 1: Representation of the numerical domain: (a) 3D view; (b) x-y plane view with main dimensions.

The numerical simulations were conducted using three different mesh systems, designed to meet the specific requirements of the employed turbulence models. The grid system features an unstructured tetrahedral mesh, except in the boundary layer, where prismatic elements are used. Fig. 2 shows the SBES mesh which consists $\sim$ 8 million cells, with 10 prismatic layers in the boundary layer, each 4×10^{-4} m thick, ensuring $y^+ > 30$. For AWMLES and WALE simulations, finer boundary layer meshes were generated, comprising 30 and 40 prismatic layers, respectively, with a first layer height of 2×10^{-6} m and a growth ratio of 1.15 on the mixing throat and diffuser walls. These configurations ensure $y^+ \leq 1$ throughout the domain. The higher resolution of the mesh parallel to the walls in the WALE simulation increases the total cell count to $\sim$ 205 million cells, compared to $\sim$ 46 million cells for the AWMLES simulation.

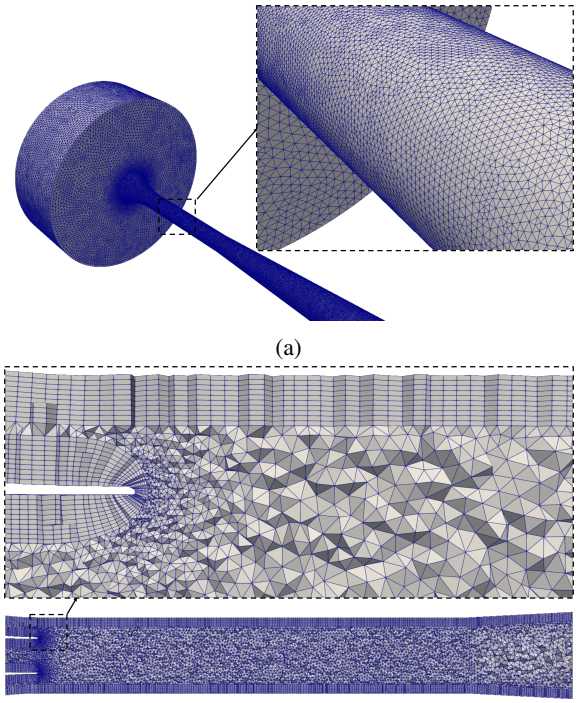

Figure. 2: Mesh grid: of (a) 3D view; (b) Longitudinal cross section views.

IV. Results and Discussions

This section evaluates the performance of the selected turbulence models in predicting key flow characteristics in Subsection IV-A and investigates the influence of the flow ratio on the internal flow field of the jet pump in Subsection IV-B.

A. Comparison of Turbulence Model Performance

The results are compared first in terms of the streamwise distribution x/d_t of the time averaged pressure coefficient $C_p = \frac{p-p_{sec.}}{\frac{1}{2}\rho v^2}$, along the centerline of the jet pump. p is the time averaged static pressure on the jet pump's wall, $p_{sec.}$ is the static pressure of the secondary inlet, v is the average velocity of the primary flow at the nozzle's outlet and d_t is the throat diameter. The SBES and AWMLES simulations are compared with the experimental data in Fig. 3 for a flow ratio equal

to $M = \frac{Q_{sec.}}{Q_{prim.}} = 1.6$, where $Q_{sec.}$ and $Q_{prim.}$ are volume flowrates of the secondary and primary flows, respectively. The numerical C_p results of both models reasonably follow the experimental data, with Mean Absolute Error (MAE) of 0.0284 for SBES and 0.0307 for AWMLES. The figure also includes the instantaneous C_p results from the WALE model. Due to the high computational cost of obtaining sufficient data for averaging, only instantaneous results are shown, which fluctuate around the averaged data from the other two models.

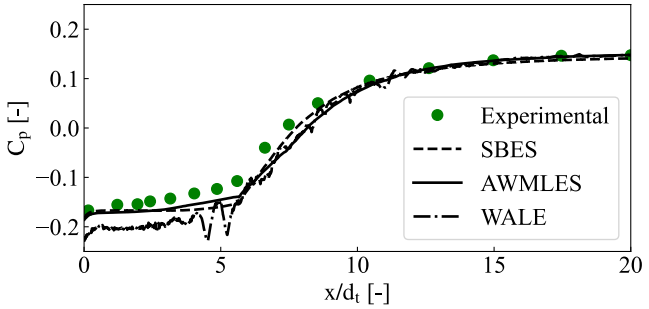

Figure. 3: Streamwise distribution of the static pressure coefficient (C_p) along the centerline of the jet pump. Comparisons between the numerical results and the experimental data [27] for M=1.6.

Fig. 4 compares the numerical mean total pressure profile $\left(p + \frac{\rho v^2}{2}\right)$, normalized by the maximum total pressure (at each section), with the experimental results at two different cross sections. The discrepancies between the numerical results and the experimental data are provided in Table I, which confirms that the results of both SBES and AWMLES models are in agreement with the experimental data.

TABLE. I: Comparison between numerical and experimental [27] total pressure profiles at two cross sections using MAE and MAPE metrics for M=1.6.

Numerical model	Cross section	MAE [-]	MAPE[a] [%]
SBES	x/d_t=4.8	0.104	28.74
	x/d_t=10.4	0.070	8.97
AWMLES	x/d_t=4.8	0.108	31.10
	x/d_t=10.4	0.058	6.65

[a]MAPE: Mean Absolute Percentage Error.

The efficiency of the jet pump ($\eta = M \times \frac{P_{\text{out}} - P_{\text{sec.}}}{P_{\text{prim.}} - P_{\text{out}}}$, where P_{out}, $P_{\text{prim.}}$, and $P_{\text{sec.}}$ are the total pressures at the outlet, primary flow inlet, and secondary flow inlet, respectively) is also used to evaluate the selected numerical models' performance. The experimental efficiency of the device operating with $M = 1.6$ is 32.60%, while the efficiencies from the SBES and AWMLES models are 34.72% and 35.53%, respectively.

Although the performances of SBES, AWMLES, and WALE models are not significantly different when compared to the available experimental data, the computational costs of AWMLES and WALE are considerably higher. Therefore, considering the balance between accuracy and computational

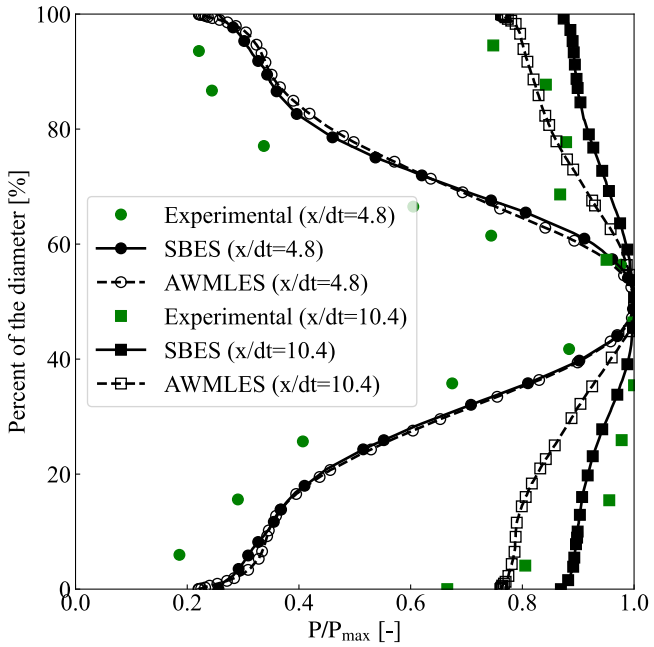

Figure. 4: Total pressure profiles at two cross sections for M=1.6. Comparisons between the numerical results and the experimental data [27].

cost, SBES is a more reasonable choice for scale-resolving simulations of the jet pump and is selected for analyzing the internal flow field across various flow ratios.

B. Effects of Flow Ratio on Internal Flow Dynamics

The instantaneous velocity magnitude contours on the mid-plane (x-y) of the jet pump at different flow ratios ($M = 0.5$, $M = 1.6$, and $M = 2.16$) are shown in Fig. 5. At all flow ratios, the formation of mixing layers is observed at the boundary of the primary jet as it exits the nozzle. These mixing layers exhibit a wavy pattern due to the appearance of Kelvin–Helmholtz instabilities. A notable distinction between the flow cases is the location of jet breakup, where the coherent jet core dissipates due to momentum transfer between primary and the secondary flow. The figure confirms that the higher the flow ratio, the further downstream the jet breakup occurs. This behavior is attributed to the lower outlet pressure required to achieve higher flow ratios (for a constant primary flow rate), which reduces the opposing pressure acting on the jet.

If the jet pump is used for mixing two fluids, the jet breakup location indicates where the fluids are effectively mixed. For low flow ratios (e.g., $M = 0.5$ as depicted in Fig. 5a), the mixing occurs earlier, allowing for a shorter device to be used. However, for higher flow ratios (e.g., $M = 2.16$ as depicted in Fig. 5c), where a larger volume of secondary flow is entrained, longer jet pumps are required to ensure sufficient mixing. It is worth noting that the efficiency of the jet pump is lower in both of extreme cases compared to when the mixing occurs at the end of the mixing throat ($M = 1.6$ shown in Fig. 5b). At low flow ratios, the reduced efficiency is due to limited

entrainment, while at high flow ratios, sudden expansion losses (as observed in [28]) affect the efficiency adversely.

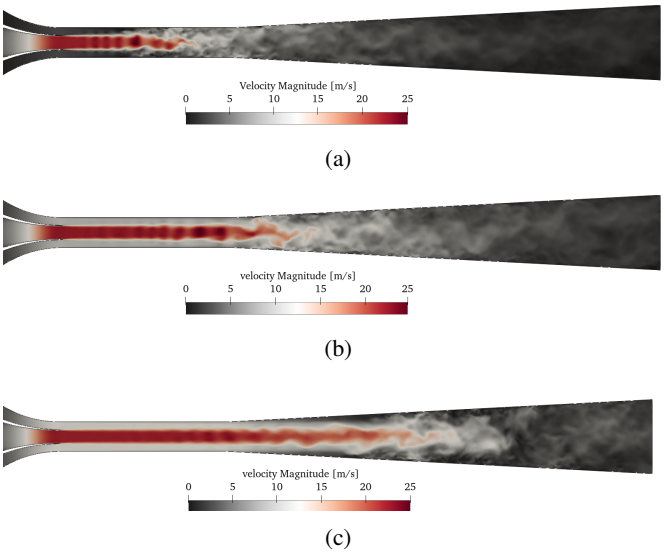

Figure. 5: Contours of the instantaneous velocity magnitude obtained by the SBES model for flow ratios equal to (a) M=0.5, (b) M=1.6 and (c) M=2.16.

Figure 6 shows the isosurfaces of positive Q-criterion. The structures are colored by the streamwise vorticity. The figure reveals distinct regions downstream of the nozzle as explained in [29]. In the initial stage near the nozzle exit, ring-like vortex structures form due to Kelvin-Helmholtz instabilities in the shear layer at the boundary between the primary jet and the secondary flow. Downstream, these vortices undergo a pairing process, merging into larger structures. Finally, in the far-field region, the vortices destabilize in the azimuthal direction, transitioning into fully 3D structures. A key observation in the jet pump is that the location where these coherent, ring-like structures break up into three-dimensional turbulence shifts further downstream as the flow ratio increases. This phenomenon is consistent with the increased jet penetration observed in the velocity magnitude contours (Fig. 5).

Figure 6 also highlights that the ring-like structures near the nozzle exhibit nearly zero rotation around the x-axis, reflecting their symmetry. However, once these rings destabilize, regions of both positive and negative rotation around the x-axis appear, marking the onset of streamwise 3D structures.

V. Conclusions

The present paper numerically investigated the internal flow field of a jet pump using three scale-resolving turbulence models: WALE, AWMLES, and SBES. Once the optimal turbulence model was selected, the influence of the flow ratio on the behavior of the device was explored.

In terms of turbulence model performance, all three investigated models provided comparable results to the experimental data. For example, the MAE of the pressure coefficient is 0.0284 for SBES and 0.0307 for AWMLES. On the other hand, SBES requires considerably less computational cost than the other models due to its ability to cover the boundary layer completely with the RANS approach. Combining these factors makes SBES a favorable choice for practical engineering problems involving high Reynolds number flows.

Analyzing the effects of the flow ratio on the internal flow field of jet pumps using instantaneous velocity field and turbulent structures revealed that higher flow ratios cause the primary jet breakup to occur further downstream. This finding is particularly important when the jet pump is used as a mixer, since mixing a larger amount of secondary flow with a constant amount of primary flow requires a longer device to be efficient.

Future works include the quantitative characterization of turbulent mixing in the jet pump by solving a passive scalar transport equation. New Particle Image Velocimetry (PIV) measurements are planned to further validate the models.

Acknowledgment

The authors appreciate the supports of the NSERC chair on industrial energy efficiency established in 2019 at Université de Sherbrooke and funded by Hydro-Québec, Natural Resources Canada and Copeland Canada Inc. All calculations were done using the clusters of the Digital Research Alliance of Canada, which is also gratefully acknowledged.

References

[1] T. Tan, J. Liu, H. Chen & W. Lu, "Review and comparison of ejectors design methods and their application," in ASME International Mechanical Engineering Congress and Exposition, vol. 8A, IMECE2014-36146, V08AT10A087, Montreal, November 14-20, 2014.

[2] J. Zhao, X. Wei, J. Zou, Y. Zhang, J. Sun & Z. Liu, "Research on performance optimization of gas–liquid ejector in multiphase mixed transportation device," Journal of Mechanics, vol. 38, pp. 22–31, 2022.

[3] H. Qian, J. Liu, M. Xu, C. Fan & Z. Duan, "Experimental Investigation on the Impact of Sand Particle Size on the Jet Pump Wall Surface Erosion," Journal of Marine Science and Engineering, vol. 12, no. 8, 1390, 2024.

[4] X. Chen, S. Wang, X. Wang, K. Chen, H. Su & M. Chen, "Experimental investigation on the convey performance and control strategy of a special annular jet pump for deep sea feeding," Aquacultural Engineering, vol. 107, 102454, 2024.

[5] S. Croquer, Y. Fang, A. Metsue, Y. Bartosiewicz & S. Poncet, "Compound-choking theory for supersonic ejectors working with real gas," Energy, vol. 227, 120396, 2021.

[6] O. Samake, N. Galanis, M. Sorin, "Thermodynamic study of multi-effect thermal vapour-compression desalination systems," Energy, vol. 72, pp. 69–79, 2014.

[7] L. Xiao, X. Long, L. Li, M. Xu, N. Wu & Q. Wang, "Movement characteristics of fish in a jet fish pump," Ocean Engineering, vol. 108, pp. 480–492, 2015.

[8] G. Besagni, "Ejectors on the cutting edge: The past, the present and the perspective," Energy, vol. 170, pp. 998–1003, 2019.

[9] I. Lima Neto, "Maximum suction lift of water jet pumps," Journal of Mechanical Science and Technology, vol. 25, pp. 391–394, 2011.

[10] T. Meakhail & I. Teaima, "Experimental and numerical studies of the effect of area ratio and driving pressure on the performance of water and slurry jet pumps," Proceedings of the Institution of Mechanical Engineers, Part C: Journal of Mechanical Engineering Science, vol. 226, no. 9, pp. 2250–2266, 2012.

[11] L.R. Sobenko, J.A. Frizzone, A.P. de Camargo, E. Saretta, & H.S. da Rocha, "Characterization of venturi injector using dimensional analysis," Revista Brasileira de Engenharia Agricola e Ambiental, vol. 23, no. 7, pp. 484–491, 2019.

[12] S. Winoto, H. Li & D. Shah, "Efficiency of jet pumps," Journal of Hydraulic Engineering, vol. 126, no. 2, pp. 150–156, 2000.

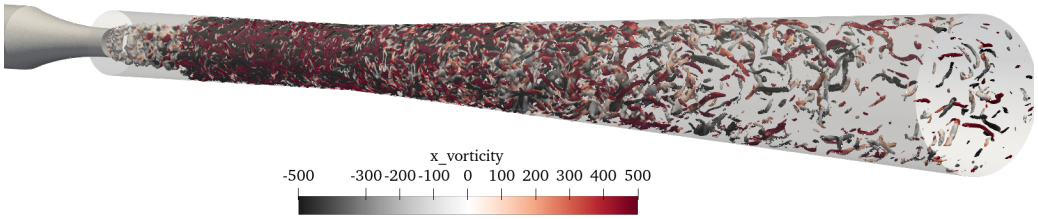

(a)

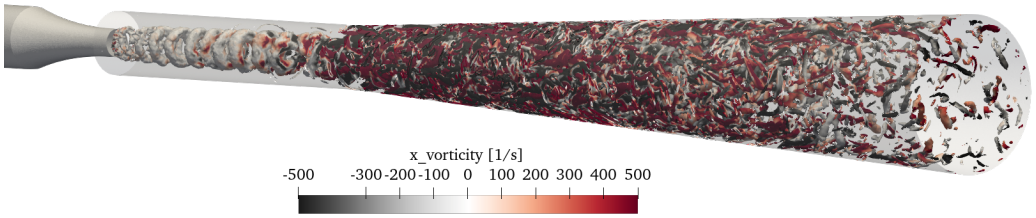

(b)

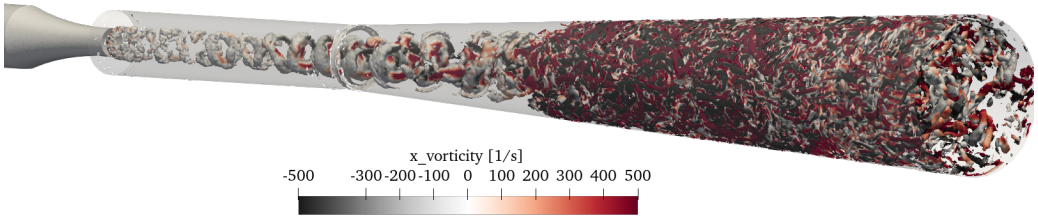

(c)

Figure. 6: Iso-surfaces of the Q-criterion colored by the streamwise vorticity achieved using the SBES model for flow ratios equal to (a) M=0.5, (b) M=1.6 and (c) M=2.16.

[13] K. Aldaş & R. Yapici, "Investigation of effects of scale and surface roughness on efficiency of water jet pumps using CFD," Engineering Applications of Computational Fluid Mechanics, vol. 8, no. 1, pp. 14–25, 2014.

[14] H. Li, X. Huang, Q. Han, Y. Yuan & B. Qi, "Numerical and experimental study on the internal flow of the venturi injector," Processes, vol. 8, no. 1, 64, 2020.

[15] X. Yang & X. Long, "Numerical investigation on the jet pump performance based on different turbulence models," IOP Conference Series: Earth and Environmental Science, 2012.

[16] B. Kim & K. Chang, "Assessment of hybrid RANS/LES models in heat and fluid flows around staggered pin-fin arrays," Energies, vol. 13, no. 14, pp. 3752, 2020.

[17] I. Celik, Z. Cehreli & I. Yavuz, "Index of resolution quality for large eddy simulations," Journal of Fluids Engineering, vol. 8, no. 1, pp. 14–25, 2005.

[18] I. Tkatchenko, N. Kornev, S. Jahnke, G. Steffen & E. Hassel, "Performances of LES and RANS models for simulation of complex flows in a coaxial jet mixer," Flow, Turbulence and Combustion, vol. 78, pp. 111–127, 2007.

[19] S. Zaheer, J. Masud & A. Shabbir, "Effect of turbulence modeling on realistic estimation of flow characteristics of liquid ejector pump," in 2018 15th International Bhurban Conference on Applied Sciences and Technology (IBCAST), 2018, pp. 658–663.

[20] M.S. Xu, X.L. Yang, X.P. Long & Q. Lu, "Large eddy simulation of turbulent flow structure and characteristics in an annular jet pump," Journal of Hydrodynamics, vol. 29, no. 4, pp. 702–715, 2017.

[21] M.S. Xu, X.L. Yang, X.P. Long, Q. Lu & B. Ji, "Numerical investigation of turbulent flow coherent structures in annular jet pumps using the LES method," Science China Technological Sciences, vol. 61, pp. 86–97, 2018.

[22] Q. Zaheer & J. Masud, "Visualization of flow field of a liquid ejector pump using embedded LES methodology," Journal of Visualization, vol. 20, pp. 777–788, 2017.

[23] F. Nicoud & F. Ducros, "Subgrid-scale stress modelling based on the square of the velocity gradient tensor," Flow, Turbulence and Combustion, vol. 62, no. 3, pp. 183–200, 1999.

[24] M.L. Shur, P.R. Spalart, M.K. Strelets & A.K. Travin, "A hybrid RANS-LES approach with delayed-DES and wall-modelled LES capabilities," International Journal of Heat and Fluid Flow, vol. 29, no. 6, pp. 1638–1649, 2008.

[25] F. Menter, "Stress-blended eddy simulation (SBES)—A new paradigm in hybrid RANS-LES modeling," In: Hoarau, Y., Peng, SH., Schwamborn, D., Revell, A. (eds) Progress in Hybrid RANS-LES Modelling. HRLM 2016. Notes on Numerical Fluid Mechanics and Multidisciplinary Design, vol. 137, Springer, 2018.

[26] T.H. Shih, W.W. Liou, A. Shabbir, Z. Yang & J. Zhu, "A new k-ε eddy viscosity model for high Reynolds number turbulent flows," Computers & Fluids, vol. 24, no. 3, pp. 227–238, 1995.

[27] N. Sanger, "Noncavitating and cavitating performance of two low-area-ratio water jet pumps with throat lengths of 5.66 diameters," NASA, Technical Report, 1968.

[28] R.G. Cunningham, "Gas compression with the liquid jet pump," Journal of Fluids Engineering, vol. 96, no. 3, pp. 203-215, 1974.

[29] A.S. Ginevsky, Y.V. Vlasov, E.V. Vlasov & R.K. Karavosov, *Acoustic Control of Turbulent Jets*. Springer Science & Business Media, 2004.